energies

MDPI

Article

# Investigation of a Co-Axial Dual-Mechanical Ports Flux-Switching Permanent Magnet Machine for Hybrid Electric Vehicles

**Wei Hua * and Ling Kang Zhou**

Received: 31 July 2015; Accepted: 14 December 2015; Published: 18 December 2015
Academic Editor: Omar Hegazy

School of Electrical Engineering, Southeast University, Nanjing 210096, China; m13601401479@163.com
* Correspondence: huawei1978@seu.edu.cn; Tel.: +86-25-8379-4152; Fax: +86-25-8379-1696

**Abstract:** In this paper, a co-axial dual-mechanical ports flux-switching permanent magnet (CADMP-FSPM) machine for hybrid electric vehicles (HEVs) is proposed and investigated, which is comprised of two conventional co-axial FSPM machines, namely one high-speed inner rotor machine and one low-speed outer rotor machine and a non-magnetic ring sandwiched in between. Firstly, the topology and operation principle of the CADMP-FSPM machine are introduced; secondly, the control system of the proposed electronically-controlled continuously-variable transmission (E-CVT) system is given; thirdly, the key design specifications of the CADMP-FSPM machine are determined based on a conventional dual-mechanical ports (DMP) machine with a wound inner rotor. Fourthly, the performances of the CADMP-FSPM machine and the normal DMP machine under the same overall volume are compared, and the results indicate that the CADMP-FSPM machine has advantages over the conventional DMP machine in the elimination of brushes and slip rings, improved thermal dissipation conditions for the inner rotor, direct-driven operation, more flexible modes, lower cogging torque and torque ripple, lower total harmonic distortion (THD) values of phase PM flux linkage and phase electro-motive force (EMF), higher torque output capability and is suitable for the E-CVT systems. Finally, the pros and cons of the CADMP-FSPM machine are highlighted. This paper lays a theoretical foundation for further research on CADMP-FSPM machines used for HEVs.

**Keywords:** co-axial; dual mechanical ports; stator permanent magnet; flux switching; brushless machines; continuously-variable transmission; hybrid electric vehicles; power splitter

## 1. Introduction

Presently, in order to conquer the disadvantages of the planet gear-based continuously-variable transmission (CVT) systems used in hybrid electric vehicles (HEVs), such as gear noise, lubrication and maintenance, a series of dual-mechanical ports (DMP) machines is proposed, and consequently, the electronically-controlled continuously-variable transmission (E-CVT) system is put forward to replace the planet gear-based system. The topology and principle of a DMP machine for HEVs was introduced in 2002, which is named the four-quadrant transducer (4QT) [1], and since then, many different topologies of 4QT-based machines have been proposed [2–4]. However, for the first time, the concept of "dual-mechanical ports electric machines" was proposed by Prof. Longya Xu in [5], where the DMP machine is comprised of three main components, namely an outer stator with evenly-configured three-phase-distributed armature windings, an outer cup-type rotor with two layers of permanent magnets (PMs) surface mounted on the inside and outside of the rotor lamination and an inner wound rotor also with evenly-configured three-phase distributed windings. Obviously, the stator and the outer rotor with the outside layer of the PMs can be regarded as an outer PM

brushless machine, and the inner wound rotor and the outer rotor with the inside layer of PMs can be regarded as an inner PM machine, while the outer PM rotor with two layers of magnets is commonly shared by the outer and inner machines. However, since the inner wound rotor has to rotate, brush and slip rings are necessary for this kind of DMP machine and results in mechanical loss and scheduled maintenance, which is unfavorable for the high-speed operation of the inner rotor. Furthermore, the thermal dissipation is a big challenge for applications in HEVs, where the ambient temperature is relatively high. In 2013, a new structure of the DMP machines was proposed in [6], which is an integration of a multi-pole fractional slot concentrated windings PM (MP-FSCW-PM) machine and a double-rotor vernier PM (DVPM) machine. The outer rotor is commonly shared by the two machines, and it has two rotors and stators. However, the extremely high frequency of back electro-motive force (EMF) will exist when the DVPM machine operates at a high speed. Recently, a novel structure of a flux-switching permanent magnet-based double-rotor machine (FSPM-DRM) was also proposed in 2014 [7], which is comprised by two individual FSPM machines with more sinusoidal phase back EMF waveforms and a higher torque density than that of the 4QT; whereas the armature windings and PMs of the inner FSPM machine are installed in the inner rotor, which will reduce the structural strength and increase the difficulty of heat dissipation; also, it still needs brushes and slip rings.

Generally speaking, the DMP machines mentioned above conquer some of the disadvantages of the planet gear-based mechanical CVT systems; however, they need brushes and slip rings, which will cause extreme mechanical loss and need regular maintenance. Figure 1a shows the structure of a conventional DMP machine-based E-CVT system, including a DMP machine with a wound inner rotor, converters and battery packs. It should be noted that the DMP machine usually consists of a stator, an inner rotor with windings and an outer rotor with windings [1] or magnets [8]. When the E-CVT system works, the internal combustion engine (ICE), which is directly connected to the inner rotor through slip rings, is controlled to operate with the most proper model of the fuel combustion point (FCP) under a certain speed, whereas the outer rotor is coupled to the drive shaft by reduction gears, and hence, the output torque and speed of the outer rotor are controlled by regulating the currents in the armature windings of the stator. Obviously, the DMP machine-based E-CVT system needs brushes, slip rings and gears, which will inevitably result in additional loss and regular maintenance.

Hence, recently, a novel topology of a co-axial dual-mechanical ports flux-switching permanent magnet (CADMP-FSPM) machine is proposed in [9], which overcomes the shortcomings existing in the previous DMP machines and provides a new concept to construct the E-CVT system. The CADMP-FSPM machine consists of an outer FSPM machine and an inner FSPM machine co-axially configured, where the inner FSPM machine is essentially an inner rotor FSPM machine and directly coupled to the ICE, and the outer FSPM machine is essentially an outer rotor FSPM machine and directly coupled to the power train of the drive system without gears. Hence, both rotors of the inner and outer FSPM machines are made of only salient pole laminations without magnets nor windings, and therefore, the brushes and slip rings are removed. However, the two stators of the outer and inner FSPM machines co-exist with a non-magnetic ring. Although in [10], a similar CADMP-FSPM machine was proposed, it exhibits such disadvantages as: (1) being more complicated since it needs a non-contact magnetic planetary gear (NC-MPG) to realize power splitting, which will cause extra loss and reduce the reliability of the whole E-CVT system; (2) the proposed FSPM machine-based E-CVT system still needs a drive motor to transmit mechanical power from the outer rotor to the powertrain through gears.

Therefore, in this paper, a comprehensive analysis and design of a CADMP-FSPM machine for practical application in the Toyota Prius is conducted in depth, where the mechanical power from the outer rotor of the outer FSPM machine is directly connected to the drive shaft without gears, *i.e.*, realizing "direct driven", as shown in Figure 1b. As can be seen, the novel E-CVT system is constructed of a CADMP-FSPM machine, a DC/DC module, two converters and a battery pack.

It should be noted that when the mechanical power due to the ICE is transferred to the inner FSPM machine by the inner rotor, the AC electrical power generated in the inner FSPM machine is then rectified into DC electrical power by the converters and stored in the battery packs. At the same time, the outer FSPM machine absorbs the power from the battery packs by a DC/AC converter to the three-phase armature windings in the stator and drives the powertrain directly. Therefore, the ICE can always operate at its optimum region independent of road conditions, and thus, the optimum HEV operation is achieved. Compared to the DMP machine-based system, obviously the CADMP-FSPM machine-based E-CVT system removes brushes, slip rings and reduction gears, and it is maintenance-free. Moreover, there is the optimal control of the inner and outer FSPM machines to realize torque and speed adjustments.

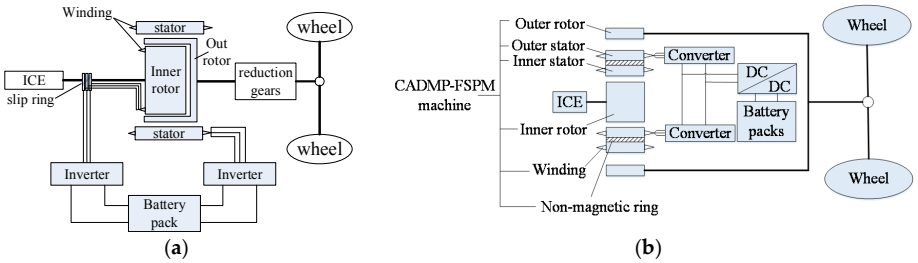


**Figure 1.** Comparison of dual-mechanical ports (DMP) machine-based and co-axial dual-mechanical ports flux-switching permanent magnet (CADMP-FSPM) machine-based electronically-controlled continuously-variable transmission (E-CVT) systems. (**a**) Scheme of an E-CVT system with a DMP machine; (**b**) Scheme of an E-CVT system with a CADMP-FSPM machine. ICE, internal combustion engine.

The detailed topology of the proposed CADMP-FSPM machine is shown in Figure 2, which is comprised by an inner rotor FSPM machine and an outer rotor FSPM machine co-axially accommodated and separated by a non-magnetic ring. As illustrated in the E-CVT system, the ICE normally works at a relatively high speed (2400 r/min to 3000 r/min) for the best fuel combustion efficiency, and hence, the inner rotor FSPM machine operates as a generator at the same constant high speed. However, since the outer rotor FSPM machine is directly coupled to the drive shaft of wheels, this means that the rated speed of the outer rotor FSPM machine is relatively low even under cruising operation mode. On the other hand, based on the design principle for the outer rotor FSPM machines [11] and the magnetic gearing effect, as pointed out in [12], specific considerations should be taken into account for the low-speed multi-pole outer rotor FSPM machine, especially at the preliminary design stage. The control system, key specifications and parameters of the inner and outer FSPM machines are to be elaborated in the following sections.

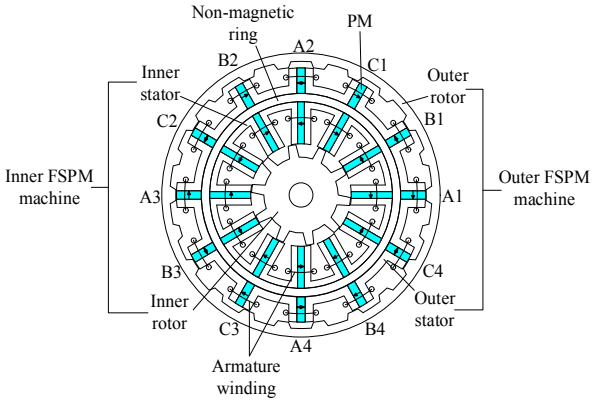


**Figure 2.** Topology of the proposed CADMP-FSPM machine (inner: 12/10, outer: 12/22).

## 2. The Control Scheme of the CADMP-FSPM Machine-Based E-CVT System

The CADMP-FSPM machine-based E-CVT system can perform six operation modes, and the control system is designed as shown in Figure 3. As can be seen, the E-CVT system has two independent speed loops, one for the inner FSPM machine and another for the outer FSPM machine. In each speed loop, there are two current loops, one for the regulation of the $q$-axis current and another for the $d$-axis current. Space vector pulse width modulation (SVPWM) method is adopted to control both machines. The energy storage system consists of the DC/DC module and the battery packs. In the control systems, the DC/AC inverters of both the inner and outer machines are connected with the DC bus. The battery packs are connected with the DC bus through the DC/DC module; thus, the battery packs can absorb energies from the DC bus or provide energies to the DC bus. The voltage across the DC-link bus is $u_{dc}$, which is also the input DC-link voltage supplied for the two AC/DC inverters of the inner and outer FSPM machines. Further, the DC current $i_2$ can be regarded as the input/output current to/from the batteries through the DC/DC module, and the DC currents $i_1$ and $i_3$ are the input/output currents to/from the AC/DC bi-direction converters of the inner and outer FSPM machines, respectively. The relationship between $i_1$, $i_2$ and $i_3$ can determine the different operation modes of the E-CVT system by controlling four power switches as shown. The E-CVT system can perform six operation modes as follows.

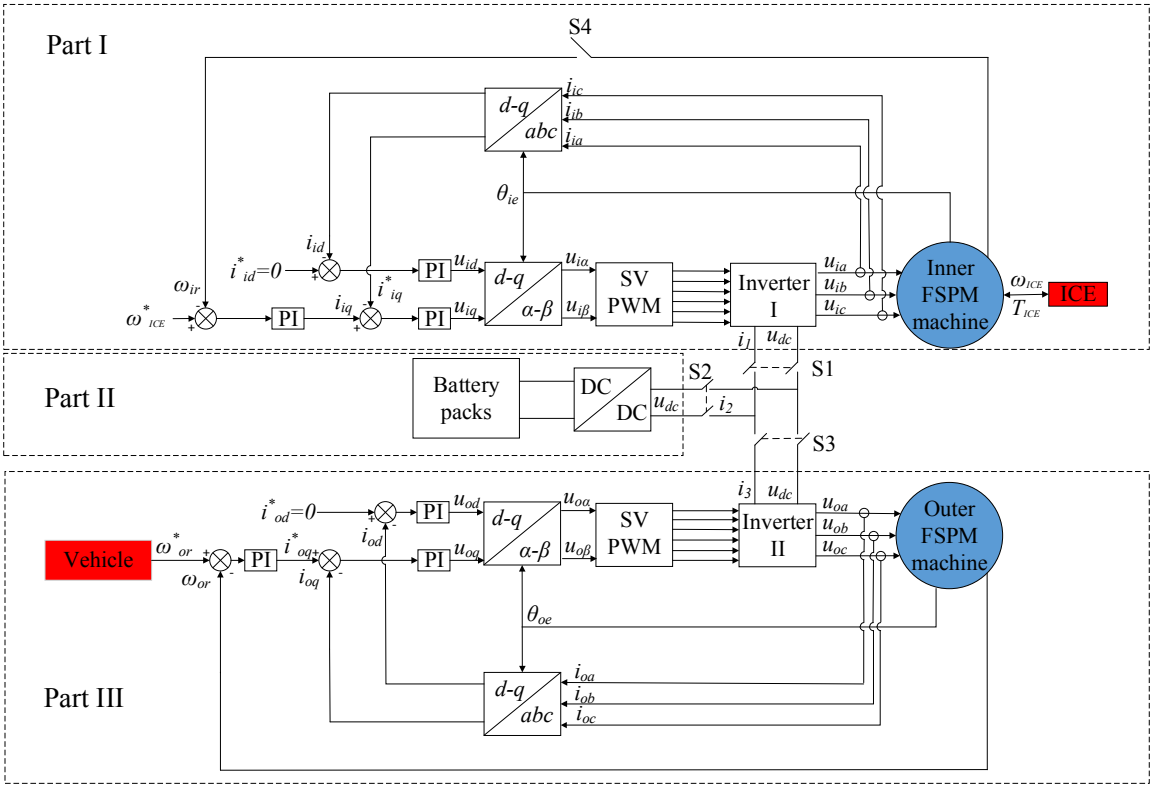


**Figure 3.** The control system of the proposed CADMP-FSPM machine-based E-CVT system.

### *2.1. The Pure Electric Launching Mode*

In the pure electric launching mode, $i_2 = i_3$ and $i_1 = 0$, where switches S2 and S3 are turned on and the others are turned off. In this manner, the control system of the inner FSPM machine stops working, and the outer FSPM machine operates as a traction motor to drive the vehicle, and the field-oriented control (FOC) or direct torque control (DTC) strategy can be adopted. Hence, the energies are only provided by the battery packs through the DC/DC module and the DC/AC

converter to the outer FSPM machine, and the power transmission path is from the battery packs to the outer FSPM machine.

### *2.2. The Hybrid Driven Mode*

In the hybrid-driven mode, $i_1 + i_2 + i_3 = 0$, and switch S4 is turned off. The closed speed loop of the inner FSPM machine is deactivated, and the ICE operates at the optimal fuel combustion point and, thus, drives the inner FSPM machine at a constant-speed mode. In this manner, the inner FSPM machine operates as a generator and provides stable AC electric energy continuously to the DC bus through the AC/DC converter. The outer FSPM machine operates as a traction motor and absorbs the energies from the DC bus through the DC/AC inverter. However, when the energy that is generated by the inner FSPM machine cannot be afforded to the outer FSPM machine, the electric energy stored in the battery packs will provide the shortage energy to the outer FSPM machine through the DC/DC module and the DC/AC converter, *i.e.*, $i_3 > i_1$. On the other hand, the battery packs will absorb the extra electrical energy when the outer FSPM machine cannot consume all of the electrical energy generated by the inner FSPM machine, *i.e.*, $i_1 > i_3$.

### *2.3. The Regenerative Braking Mode*

In the regenerative braking mode, $i_2 = i_1 + i_3$, which means that the outer FSPM machine runs as a generator when the vehicle is breaking, and the electric energy that is converted from kinetic energy is translated into the battery packs through the AC/DC converter and the DC/DC module. Meanwhile, the inner FSPM machine runs as a generator or standstill according to the situation.

### *2.4. The Engine Cranking Mode*

In the engine cranking mode, $i_1 = i_2$, $i_3 = 0$, and switch S3 is turned off. In this manner, both the outer FSPM machine and the ICE do not work, while the inner FSPM machine operates as a traction motor and drives the ICE to the starting speed $\omega^*_{ICE}$. Hence, the battery packs will provide energy to the inner FSPM machine through the DC/AC inverter, the DC bus and the DC/DC module.

### *2.5. The Pure Charging Mode*

In the pure charging mode, $i_1 = i_2$, $i_3 = 0$, and switches S3 and S4 are turned off. In this manner, the outer FSPM machine stops working, and the inner FSPM machine is driven by the ICE at a constant speed and operates as a generator to provide energy to charge the battery packs. Hence, the energy will be transferred to the battery packs through the AC/DC converter, the DC bus and the DC/DC module.

### *2.6. The Cruising Operation Mode*

In the cruising operation mode, $i_1 = i_3$, $i_2 = 0$, and switch S2 is turned off. In this manner, the inner FSPM machine is driven by the ICE and operates as a generator to provide energy, and the outer FSPM machine operates as a traction motor to drive the vehicle. Hence, the inner FSPM machine will generate the electric energy and supply the necessary power for the outer FSPM machine to drive the vehicles running at a constant high speed through the AC/DC and DC/AC converters. It should be noted that in the hybrid-driven mode, the battery packs will provide insufficient energy or absorb the redundant energy according to the different speeds of the vehicles, whereas in the cruising operation mode, both the ICE and vehicle are operated at a constant speed, respectively. Hence, the mechanical power needed for the vehicle is almost unchanged and can be supplied by the ICE through the CADMP-FSPM machine indirectly.

The small signal z-domain method could be adopted to design the controllers if Inverter I and Inverter II connect with three-phase symmetric loads, such as pure resistive and inductive loads. Considering the equivalent delays and bandwidths of current sensors, current sampling and

conditioning circuits, the ADC sampling circuits, the delay of the inverters, the insulated gate bipolar transistor (IGBT) drivers and the dead-zone of the DSP pulse-width modulation (PWM) triggers, the classical control theory of linear systems can be adopted to analyze the system, then the small signal z-domain method can also be adopted to design the controllers. However, in the proposed E-CVT system, the loads which are connected with Inverter I and Inverter II are the inner and outer FSPM machines, and the mathematical models of both machines are complex and nonlinear. The magnetic fields of both machines will change when the load torques vary, which will influence the *dq*-axes' inductances and, consequently, the *dq*-axes' voltage equations, due to couplings. Thus, both speed response and disturbance rejections of the control system should be considered for the design of the controllers. As the sampling times of the current loop and speed loop are different, the multi-rate digital control method should be adopted, and the theory of the multi-rate digital control is still under research currently. The control system in this paper involves three control models, including a DC/DC bi-directional module control model and two control models of the inverters. Furthermore, considering the power flows between the three models, the control models of the inverters of the control system are much more complex, and the PI controllers that are adopted in the paper are just typical controllers.

## 3. Design and Optimization of the CADMP-FSPM Machine

In this section, the design process and optimization of the CADMP-FSPM machine are presented in detail. Since the CADMP-FSPM machine is proposed as a dual-mechanical ports machine to realize power splitting in HEVs, the inner FSPM machine is directly coupled to the ICE for high-speed operation, and the outer FSPM machine is connected to the transmission system of the wheels through differentials and clutches for low-speed operation. Hence, for the three-phase CADMP-FSPM machine, the inner machine is chosen to employ a conventional 12 stator slots/10 rotor poles FSPM machine with an inner rotor and an outer stator [13]. However, for the outer machine, since it is directly coupled with the powertrain system of the vehicle and is controlled by the speed of the wheels, the electromagnetic pole pair number of the rotor should be larger than that of the inner machine. According to the recommended equation derived for an outer rotor structure, the outer rotor pole number can be determined as [14]:

$$P_{ro} = P_{so}\left(2 \pm \frac{k}{2m}\right) \tag{1}$$

where $P_{ro}$ and $P_{so}$ are the rotor pole number and stator slot number of the outer FSPM machine, respectively, $m$ is the phase number and $k$ is a positive integer. Here, $P_{so}$ = 12, $m$ = 3, $k$ = 1 and, thus, $P_{ro}$ = 22 [15]. It should be noted that for the CADMP-FSPM machine discussed in this paper, the stator slot numbers of both the inner and outer machines are designed as 12, which is analyzed in depth to realize the de-coupling between the two stators connected by a non-magnetic ring.

As shown in Figure 2, a pair of PMs of the same polarity are sandwiched between the U-shape iron cells in the inner and outer stators correspondingly. In addition, since the inner and outer stators have the same 12 slots and 12 pieces of magnets, the magnetic coupling between the inner and outer FSPM machines is probably a challenge when the non-magnetic ring is not thick enough. As can be seen from Figure 4a,b when the outer rotor of the outer FSPM machine is at the same position, the phase PM fluxes due to the above magnets linking Coil 1 of the outer FSPM machine are identical. However, as the inner rotor of the inner FSPM machine moves from Position A (Figure 4a) to Position B (Figure 4b), due to the different magnetic reluctances of the distinct magnetic circuits composed of the outer rotor, outer stator, non-magnetic ring, inner stator and inner rotor, the distributions of the PM fluxes due to the magnets below are different, and consequently, the resultant PM fluxes linking in Coil 1 of the outer FSPM machine have different amplitudes based on the well-known "minimum reluctance principle". Similarly, keeping the inner rotor of the inner FSPM machines and the two stators at the same positions, the combined PM fluxes due to both the magnets above and

below linking Coil 2 of the inner FSPM machine are different when the outer rotor of the outer FSPM machine moves from Position C (Figure 4c) to Position D (Figure 4d).

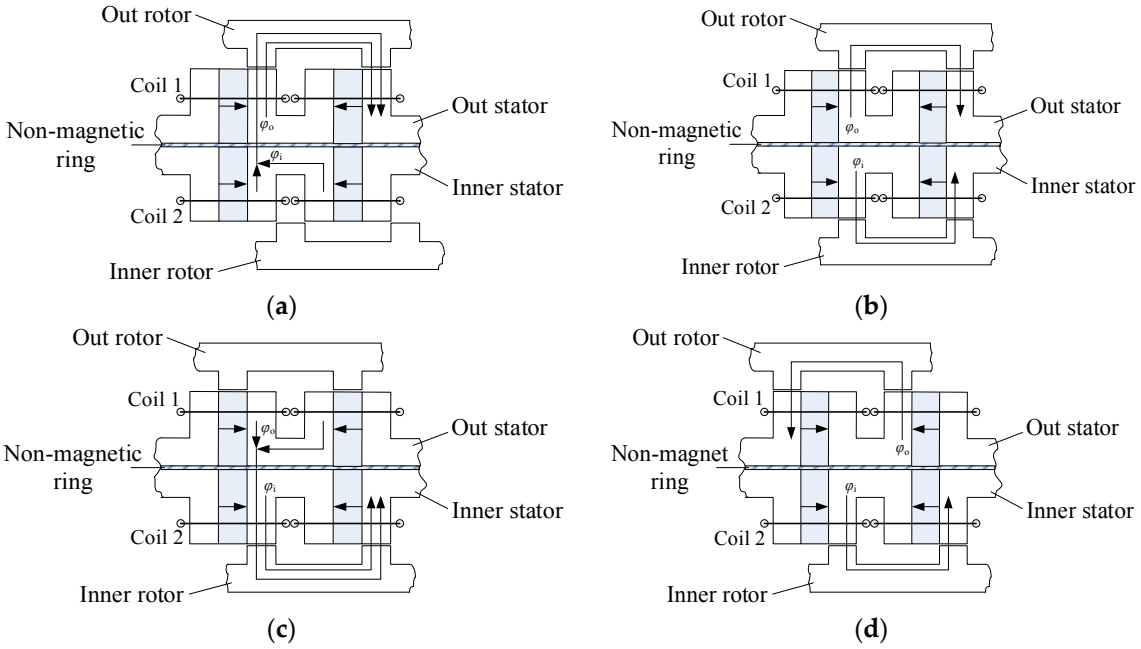


**Figure 4.** Principles of magnetic couplings. (**a**) Position A; (**b**) Position B; (**c**) Position C; (**d**) Position D.

The above analysis indicates that the non-magnetic ring plays an important role in the magnetic coupling between the inner and outer stators. If the ring is not thick enough, the amplitudes of the phase PM flux linkage in the armature windings of both the inner and outer FSPM machines will vary according to the relative positions of the inner and outer rotors. In order to reduce the magnetic couplings, an appropriate thickness of the non-magnetic ring must be optimized. On the other hand, obviously, the power (torque) density of the CADMP-FSPM machine is relative to the thickness of the non-magnetic ring. According to the principle that the magnetic flux lines flow along the minimum reluctance path, the optimal thickness of the non-magnetic ring should be equal to the thickness of the thicker magnet width of the inner and outer stators in the magnetized direction. Moreover, considering the core saturation, the non-magnetic ring should be designed carefully.

For quantified analysis, a non-magnetic ring thickness factor $k_{rt}$ is defined as $k_{rt} = h_r/h_{PM}$, where $h_r$ is the radial thickness of the non-magnetic ring and $h_{PM}$ is the thickness of the thicker magnet of both stators in the magnetized direction. Considering that the $d$-axis PM flux is unchanged in theory, hence, the degree of the magnetic couplings can be quantified by evaluating the phase PM flux pulsation of the inner FSPM machine when only the outer FSPM machine rotates, and the PM flux ripple $k_{ripple}$ is given by,

$$k_{ripple} = \varphi_{p-p}/\varphi_{ave} \quad (2)$$

where $\varphi_{p-p}$ and $\varphi_{ave}$ are the peak-to-peak and average values of the $d$-axis PM flux linkage of the inner machine when the inner machine rotor is static whilst the outer machine rotor rotates. In this way, an optimization on the thickness of the non-magnetic ring is explored, and the results are shown in Table 1. As can be seen, the magnetic coupling and the power destiny can be reduced with the thicker non-magnetic ring, which agrees with the theoretical predictions. When the $d$-axis PM flux ripple value is less than 1%, it can be considered that the magnetic coupling effect is negligible, so the optimal value of $k_{rt}$ is determined as 1.8.

**Table 1.** PM flux pulsations of the *d*-axis of the inner FSPM machine and the power density of the CADMP-FSPM machine ($J_{si} = J_{so} = 5$ A/mm$^2$, $n_{im} = 2400$ r/min and $n_{om} = 580$ r/min) with different $k_{rt}$.

| $k_{rt}$ | PM Flux Ripple of *d*-Axis (%) | Power Density (kW/m$^3$) |
|---|---|---|
| 1 | 1.44 | 1640 |
| 1.2 | 1.26 | 1599 |
| 1.4 | 1.12 | 1550 |
| 1.6 | 1.00 | 1505 |
| 1.8 | 0.90 | 1489 |
| 2 | 0.81 | 1415 |

## 4. Comparison of the CADMP-FSPM Machine and a Conventional DMP Machine

As shown in Figure 5, a conventional DMP machine, which is designed to replace the planet gear-based CVT in the Toyota Prius, is adopted to compare to the CADMP-FSPM machine discussed in this paper. It can be seen from Figure 5 that the DMP machine is comprised by an inner wound rotor, an outer PM rotor with two layers of magnets and a regular stator with three-phase distributed armature windings. The inner wound rotor and the outer PM rotor constitute the inner machine, whereas the outer PM rotor and stator constitute the outer machine. The key dimensions of the two machines are optimized, and the size parameters are listed in Tables 2 and 3 respectively. As can be seen, the DMP machine and the CADMP-FSPM machine have the same outer diameter and axial length, *i.e.*, the same volume (280 mm × 200 mm).

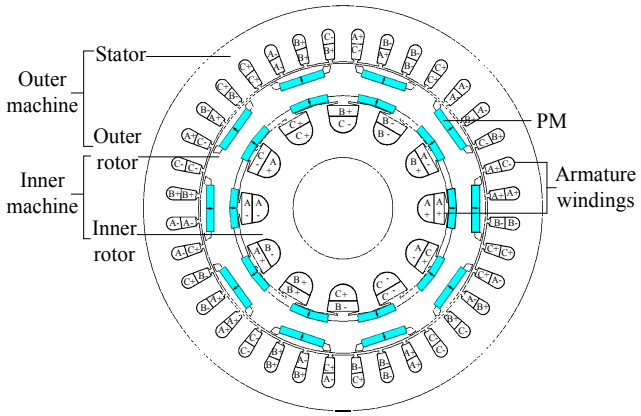


**Figure 5.** Topology of a conventional DMP machine for the Toyota Prius.

**Table 2.** Size parameters of the CADMP-FSPM machine.

| Items | Outer Rotor | Outer Stator | Inner Rotor | Inner Stator | Non-Magnetic Ring |
|---|---|---|---|---|---|
| Outer diameter (mm) | 280 | 253 | 85.575 | 117.5 | 202 |
| Inner diameter (mm) | 252 | 202 | 25 | 86.975 | 117.5 |
| Slot/pole numbers | 22 | 12 | 10 | 12 | - |
| Phase turn number | - | 6 | - | 9 | - |
| Axial length (mm) | 200 | 200 | 200 | 200 | 200 |

**Table 3.** Size parameters of the DMP machine.

| Items | Inner Rotor | Outer Rotor | Stator |
|---|---|---|---|
| Outer diameter (mm) | 148 | 201 | 280 |
| Inner diameter (mm) | 70 | 156 | 203 |
| Slot/pole numbers | 12 | 10 | 36 |
| Phase turn number | 6 | - | 2 |
| Axial length (mm) | 200 | 200 | 200 |

### *4.1. Phase Permanent Magnet Flux Linkage and Electromotive Force*

The phase PM flux linkage of the CADMP-FSPM machine and the DMP machine can be calculated by Equation (3), where, $N_{ph}$ is the stator armature winding turns per phase, $\Phi_m$ is the peak phase PM flux, $B$ is the air-gap flux density due to magnets only and $S$ is the effective cross-sectional area of the stator teeth per phase. It is worth noting that $B$ is the average value of the air gap flux density around the cross-sectional area of the stator teeth per phase, so Equation (3) can be rewritten as Equations (4) and (5) according to the structures of the CADMP-FSPM machine and the DMP machine, respectively. In Equation (4), the subscript $C$ represents the components of the CADMP-FSPM machine; hence, $B_C$ is the average value of the open-circuit air gap flux density around the cross-sectional area of the stator teeth per phase; $arc_{Csteeth}$ is the radian of single teeth per phase; $l$ is the axial length; $P_{Cs}$ is the stator slot number; and $R_{Cair-gap}$ is the radius of the circumference of the air gap. In Equation (5), the subscript $D$ represents the components of the DMP machine, and the rest of Equation (5) is similar to Equation (4). The winding turns per phase are taken as one turn before the winding turn number is determined.

$$\varphi = N_{ph}\phi_m = N_{ph}BS \tag{3}$$

$$\varphi_C = N_{Cph}B_C S_C = N_{Cph}B_C l\left(arc_{Csteeth}\frac{P_{Cs}}{m}R_{Cair-gap}\right) \tag{4}$$

$$\varphi_D = N_{Dph}B_D S_D = 2N_{Dph}B_D l(arc_{Dsteeth}\frac{P_{Ds}}{m}R_{Dair-gap}) \tag{5}$$

The air gap flux density waveforms due only to the magnets of the CADMP-FSPM machine and the DMP machine are shown in Figure 6a,b respectively. As can been seen from Figure 6, the peak value of the CADMP-FSPM machine is higher than the DMP machine due to the flux focus effect in FSPM machines [16]. It is worth noting that there are two kinds of peak values in the air gap flux density waveforms of the CADMP-FSPM machines, where one is called the "local peak value" and the other is called the "absolute peak value", due to the intersections between the rotor teeth and the stator teeth edges. However, the local peak value corresponds to the true peak value of the phase PM flux (flux linkage) in FSPM machines and is more important [17]. In addition, as can been seen from Figure 6, the peak value of the outer and inner machine of the CADMP-FSPM machine is 1.7 T and 2 T respectively, whereas the corresponding values of the DMP machine are only 1 T and 0.6 T, respectively, which indicates that the saturation of the CADMP-FSPM machine is more serious.

Further, the phase PM flux linkage per turn (*i.e.*, PM flux) waveforms of the CADMP-FSPM machine and the DMP machine are shown in Figure 7a,b respectively. Then, a fast Fourier transform (FFT) method is applied, and the relative harmonics analysis results are shown in Figure 7c,d where the phase PM flux THD (total harmonic distortions) values of the inner machines of the CADMP-FSPM and DMP machines are 0.75% and 5.96%, respectively, whereas for the two outer machines, they are 1.07% (CADMP-FSPM machine) and 2.40% (DMP machine), respectively.

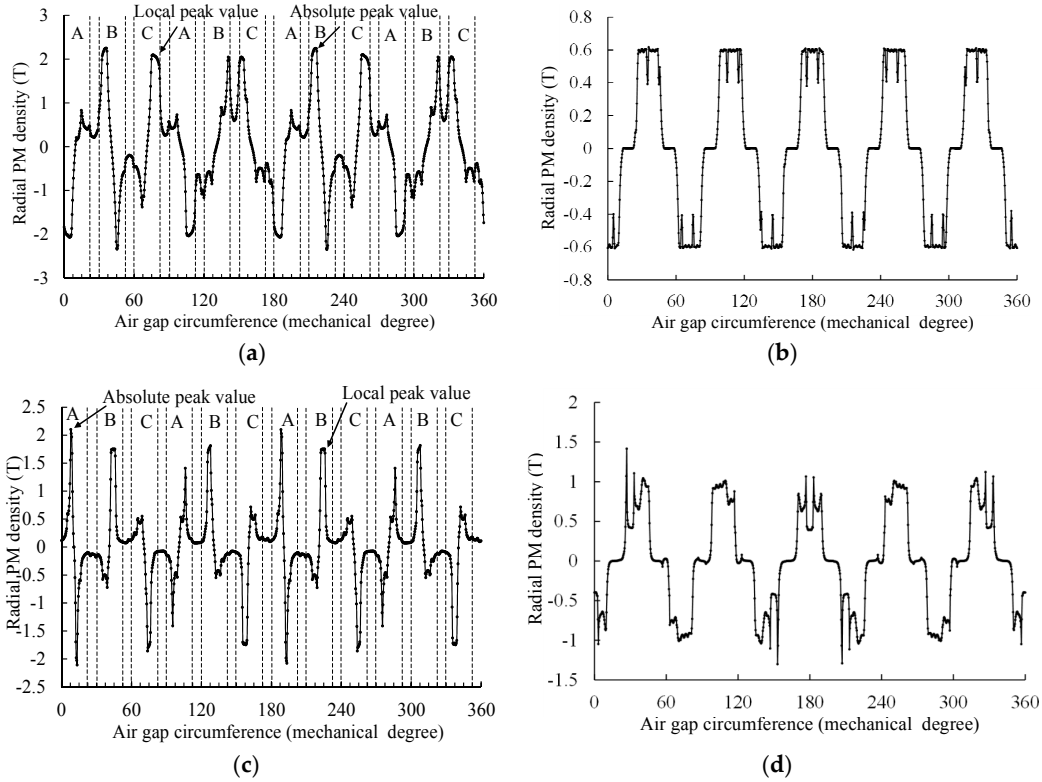


**Figure 6.** Open-circuit air gap flux density distributions of the two machines due to magnets only. (**a**) Inner FSPM machine of the CADMP-FSPM machine; (**b**) Inner machine of the DMP machine; (**c**) Outer FSPM machine of the CADMP-FSPM machine; (**d**) Outer machine of the DMP machine.

The corresponding phase electro-motive force (EMF) per turn of the CADMP-FSPM machine and the DMP machine can be calculated by Equation (6), where, $\omega_r$ is the mechanical rotation speed of the machine, $\theta_r$ is the mechanical degree of the rotor and $P_r$ is the electromagnetic pole pair number. The phase EMF per turn waveforms at 2400 r/min of the two inner machines are shown in Figure 7e; the phase EMF per turn waveforms at 580 r/min of the outer FSPM machine and the phase EMF per turn waveforms at 2500 r/min of the outer machine of the DMP machine are shown in Figure 7f. Similarly, the FFT results are shown in Figure 7g,h where the THD values of both inner machines are 2.51% and 6.86%, respectively, whereas for the outer machines, they are 3.35% and 8.51%, respectively. Furthermore, the simulation results agree with the theoretical analysis above.

As the DC-link voltage is 330 V, the winding turns per phase of two inner machines are the same, *i.e.*, six; whereas the winding turns per phase of the outer machine are nine (CADMP-FSPM machine) and two (DMP machine), respectively. In addition, a comprehensive comparison between the phase PM flux linkage and EMF characteristics considering the winding turns per phase are listed in Table 4. It can be seen that the fundamental amplitudes of both phase PM flux linkage and phase EMF (both inner machines at 2400 r/min, the outer FSPM machine at 580 r/min, the outer machine of the DMP machine at 2500 r/min) of the CADMP-FSPM machine are smaller than those of the DMP machine.

$$e_{mp} = -N_{ph}\omega_r P_r \Phi_m \sin(P_r\theta_r) = -E_m \sin(P_r\theta_r) \quad (6)$$

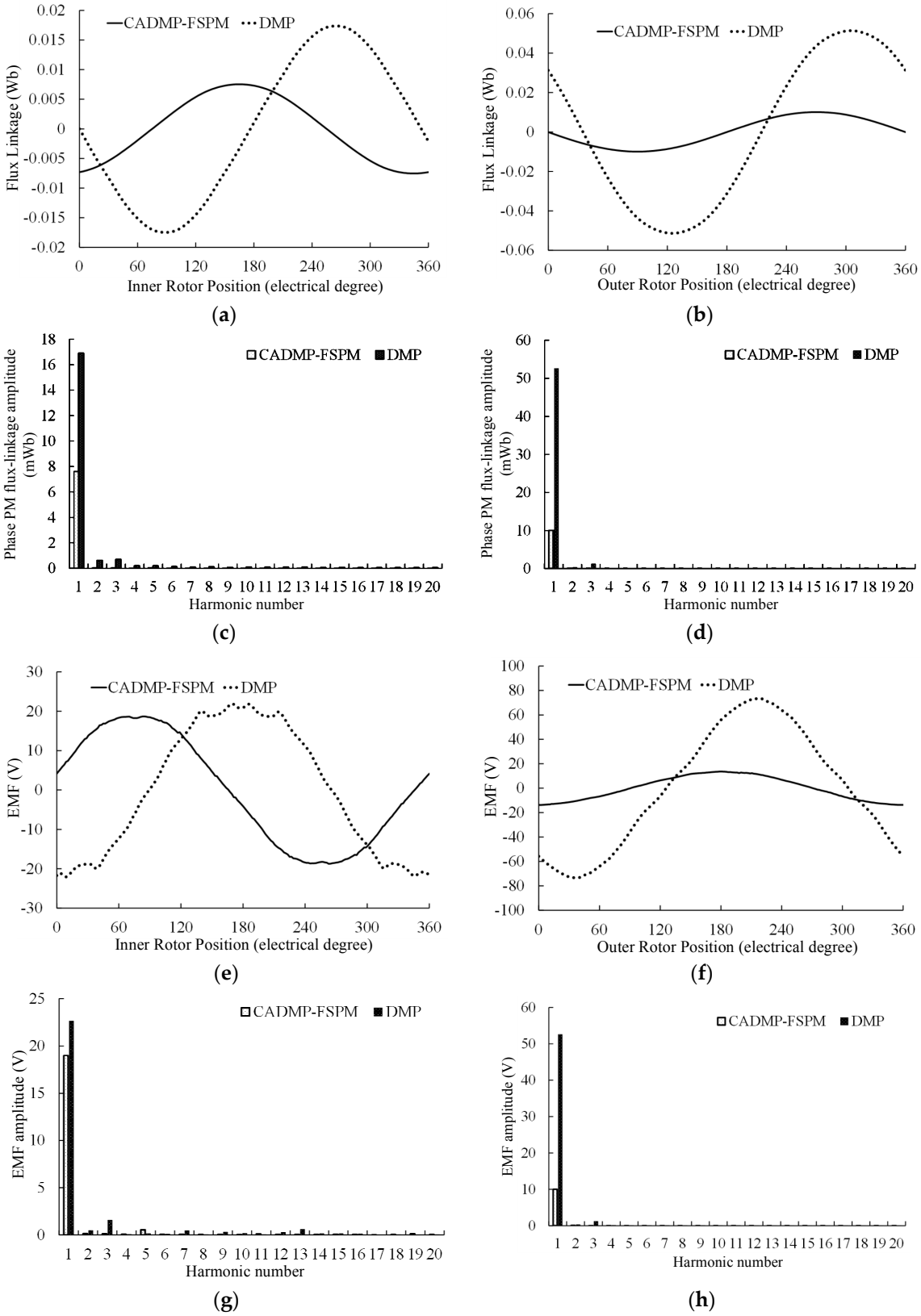


**Figure 7.** Phase PM fluxes and electro-motive forces (EMFs) per turn of two machines. (**a**) Phase PM flux waveforms of two inner machines; (**b**) Phase PM flux waveforms of two outer machines; (**c**) The phase PM flux FFT results of two inner machines; (**d**) The phase PM flux FFT results of two outer machines; (**e**) Phase EMF per turn waveforms of two inner machines; (**f**) Phase EMF per turn waveforms of two outer machines; (**g**) The phase EMF FFT results of two inner machines; (**h**) The phase EMF FFT results of two outer machines.

### *4.2. Cogging Torque*

The cogging torque waveforms of the two inner machines and the two outer machines are shown in Figure 8a,b respectively. Since the FEA software used for predicting the electromagnetic performance in the paper has no periodical mesh function, the mesh is rough, and hence, the cogging torques are not periodical. However, as analyzed in [18], the cogging torque waveform in the FSPM machine is periodical, as shown in Equation (7) below, where $C_{cog}$ is the electrical degree of one cogging torque cycle and $N_{cog}$ is the least common multiple of stator slots and rotor poles. This is also true for the interior PM (IPM) machine used in the DMP [19]. However, for the outer machine of the DMP machine, as the outer rotor is shared by both inner and outer machines, the cogging torque of the outer machine is superimposed by the cogging torques of both inner and outer machines, which causes the cogging torque cycle to be equal to the cycle of the inner machine of the DMP machine. On the other hand, it can be seen that the peak-to-peak values of the cogging torque of the inner machines of the CADMP-FSPM machine and the DMP machine are 2.76 Nm and 18.75 Nm, respectively, which means only 14.72% of that of the DMP machine. For the two outer machines, they are 15.58 Nm and 17.71 Nm, respectively, and almost the same level.

$$C_{cog} = 360^{\circ}/N_{cog} \tag{7}$$

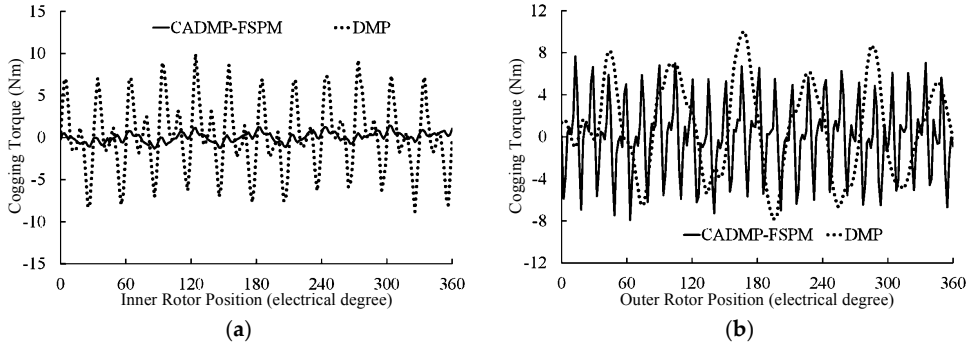


**Figure 8.** Cogging torque waveforms of two machines. (**a**) Inner machines; (**b**) Outer machines.

### *4.3. Winding Inductances*

The winding self-inductance and mutual inductance waveforms of the two machines are compared in Figure 9. since the three-phase windings are symmetrical in both the inner and outer machines for the two machines, only one phase (Phase A) is analyzed here. It can be found from Figure 9a that for the inner machine of the DMP machine, the self-inductance waveform is constant with respect to the inner rotor position region from 0° to 180° in electrical degrees, whereas for the inner machine of the CADMP-FSPM machine, the self-inductance waveform is close to a sinusoidal distribution, and the frequency of the waveform is only one in a whole electrical period, which agrees with the normal FSPM machines. On the other hand, for the two outer machines, as shown in Figure 9b, the self-inductance waveforms of both machines exhibit sinusoidal distributions with different frequencies, namely one for the CADMP-FSPM machine and two for the DMP machine due to the distinct magnet locations.

From Figure 9c–f, it can be found that the mutual inductances ($M_{ab}$ and $M_{ac}$) of the inner machine of the DMP machine are almost equal to zero during the whole electrical period, which means that the mutual couplings between the phases of the inner machine are negligible, whereas for the outer machine of the DMP machine, the variation frequencies of the mutual-inductance waveforms are also equal to two, as the self-inductance. However, for the inner and outer machines of the CADMP-FSPM machine, the mutual inductance waveforms are all close to being sinusoidal, and the frequency is only one, which is the feature of the stator PM machines [13]. The detailed results of the winding inductances of both machines are listed in Table 4.

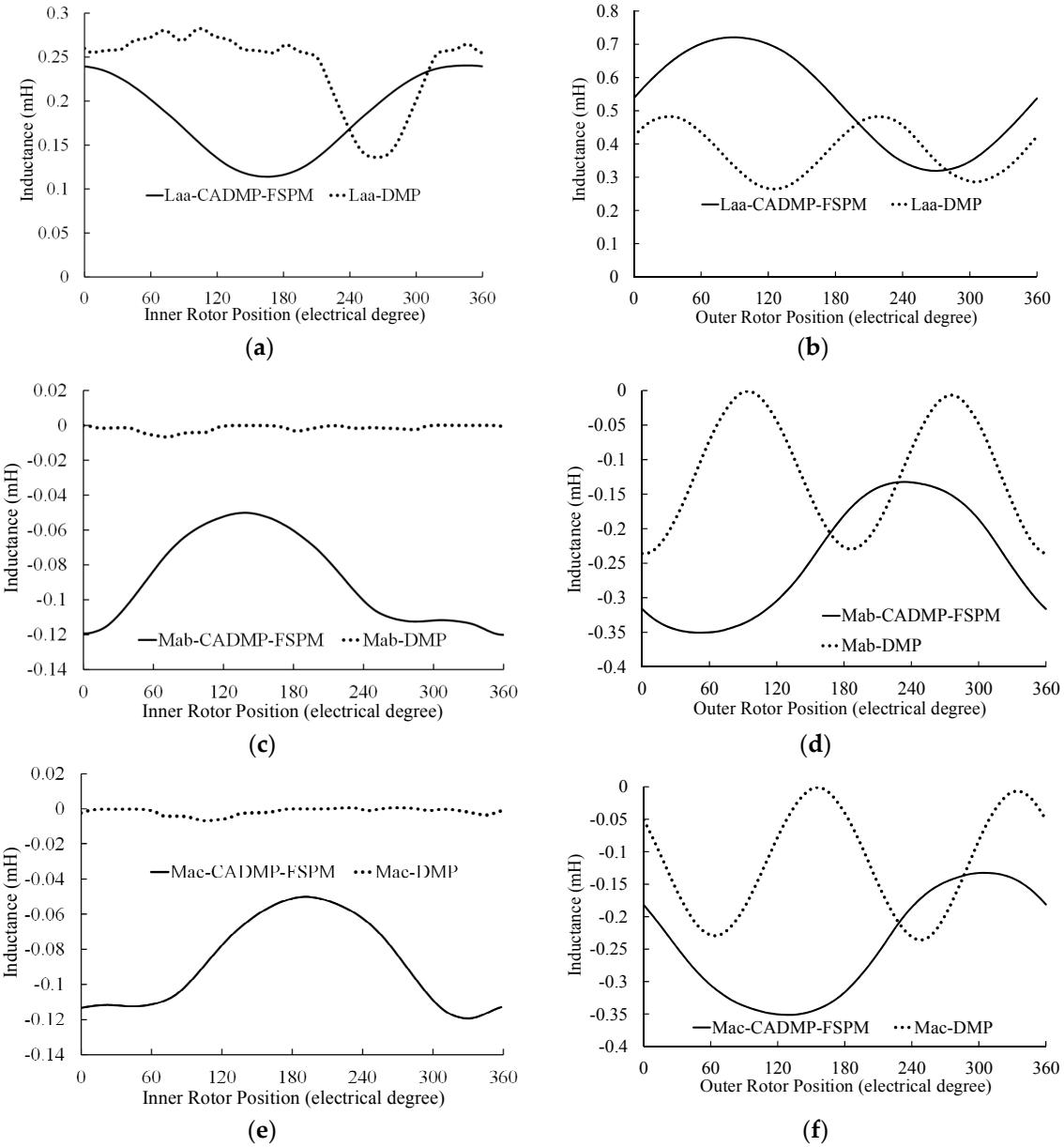


**Figure 9.** Winding self-inductance and mutual inductance of two machines. (**a**) $L_{aa}$ of inner machines; (**b**) $L_{aa}$ of outer machines; (**c**) $M_{ab}$ of inner machines; (**d**) $M_{ab}$ of outer machines; (**e**) $M_{ac}$ of inner machines; (**f**) $M_{ac}$ of outer machines.

### *4.4. Electromagnetic Torque and Power Density*

The electromagnetic torque of PM excited machines normally consists of three components, namely the PM-excited torque $T_{pm}$, the reluctance torque $T_r$ due to the difference between the $dq$-axes' inductances and cogging torque $T_{cog}$, as expressed by Equation (8).

$$T_{em} = T_{pm} + T_r + T_{cog} = \frac{3}{2} P_r \left[ \psi_m i_q + \left( L_d - L_q \right) i_q i_d \right] + T_{cog} \tag{8}$$

To compare the torque capability of the CADMP-FSPM and the DMP machines, the control arithmetic, which can produce maximum torque, should be employed. Figure 10a shows the relationship between torque and current angles, and as can be seen, the reluctance torques of the inner and outer FSPM machines of the CADMP-FSPM machine and the inner machine of the DMP

machine are negligible. Therefore, these three sub-machines are operated under $i_d = 0$ control in this paper. However, the reluctance torque in the outer machine of the DMP machine is high; hence, the maximum torque per ampere (MTPA) control arithmetic is adopted. For both the CADMP-FSPM and DMP machines, an armature current density of $J_{sai}$ = 6.4 A/mm$^2$ is injected into the inner machines, and an armature current density of $J_{sao}$ = 5 A/mm$^2$ is injected into the outer machines. It should be noted that the electromagnetic torque of the outer rotor of the DMP machine is provided jointly by both the inner and outer machines; therefore, the output torque of the outer machine of the DMP machine should be the combined torque when comparing the output torque of outer machines. Therefore, the torque of the outer machine of the DMP machine is transmitted to the drive shaft through a reduction gear to boost the drive torque, so the torque of the drive shaft of the DMP machine-based E-CVT system is introduced for a more fair comparison of the output torque capability of the two machines, where the reduction gear ratio used in the DMP machine-based system is 1.23.

The electromagnetic torque waveforms of the inner and outer machines are shown in Figure 10b,c, respectively. The detailed results are listed in Table 4. It can be seen that the torque ripples of the inner machines of the CADMP-FSPM machine are smaller than that of the DMP machine, whereas the torque ripples of the outer machines of both machines are similar. In addition, the averaged electromagnetic torques of both the inner and outer machines of the CADMP-FSPM machine are higher than those of the DMP machine due to the higher electromagnetic pole pair number and the larger slot area. It is worth mentioning that the average torque of the outer machine of the CADMP-FSPM machine is even higher than the output torque of the drive shaft of the DMP machine-based E-CVT system, which means that the torque output capability of the CADMP-FSPM machine can be in full compliance with the requirements of the HEVs, and the reduction gears can be removed.

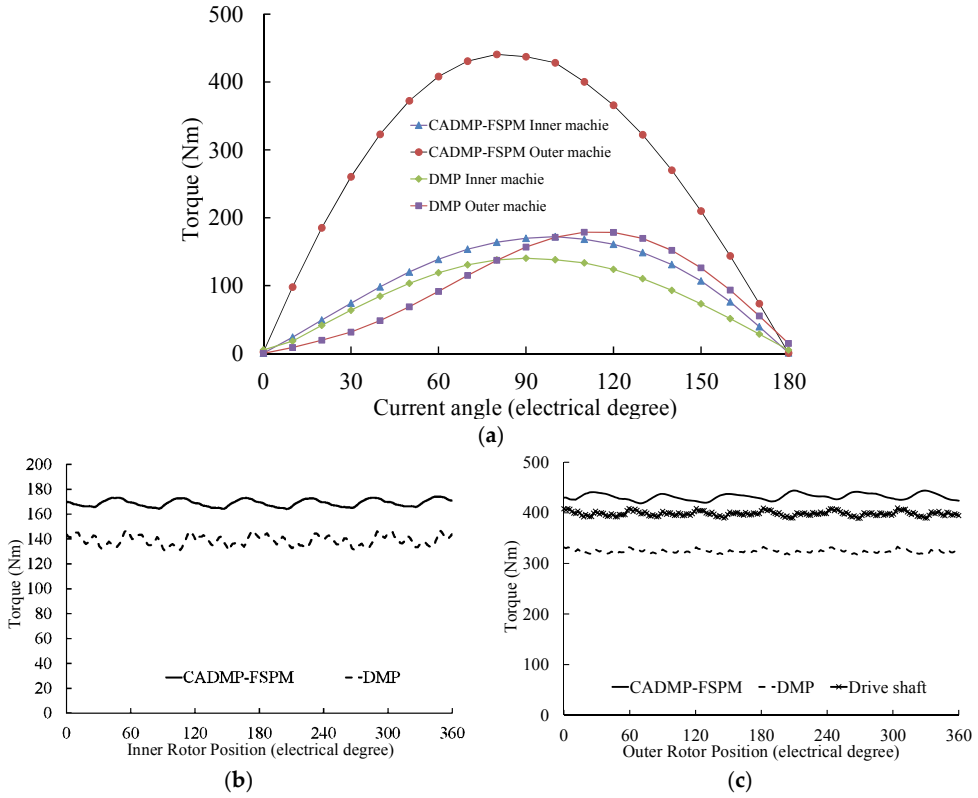


**Figure 10.** Electromagnetic torque waveforms of two machines. (**a**) Relationship between torque and current angles; (**b**) Inner machines; (**c**) Outer machines and the drive shaft of the DMP machine-based E-CVT system.

Power density is another key performance for the E-CVT systems used in HEVs. For the two machines, the power density can be expressed by Equation (9), where $P_{total}$ is the rated power of the machine and $V$ is the volume of the machine, respectively.

Since the inner machines are directly connected with the ICE running at a constant speed for optimal fuel combustion point operation, the rated speed of the inner machines of both machines is the same as 2400 r/min. However, since the outer machine of the CADMP-FSPM machine is directly connected to the drive system without gears, its rated speed is chosen as 580 r/min because of the higher number of pole pairs of the outer FSPM machine, which is lower than that of the DMP machine (2500 r/min). The detailed power density, as well as the core loss and copper loss at rated operating conditions of both machines are listed in Table 4. As can be seen, the loss of the CADMP-FSPM machine is higher than that of the DMP machine because of the higher frequency and larger slot areas. However, the total power of the CADMP-FSPM machine is lower than that of the DMP machine due to the lower rated speed of the outer machine and the existence of the non-magnetic ring; thus, the power density of the CADMP-FSPM machine is slightly lower than that of the DMP machine. On the other hand, since the reduction gears are removed in the CADMP-FSPM machine-based E-CVT system, the whole power density of the powertrain of the drive systems should be improved. In addition, the non-magnetic ring consists of non-conducting magnetic materials, such as aluminum, so the cooling system will be placed and connected with the holes made on the non-magnetic ring. In addition, as can be seen from Figures 2 and 5 the CADMP-FSPM machine does not have any windings on the inner rotor, whereas the DMP machine has windings on the inner rotor, and obviously, the windings will create heat when injecting armature currents. Moreover, the existence of windings will squeeze the cooling space. In that case, the CADMP-FSPM machine has the advantage of improved thermal dissipation conditions for the inner rotor.

$$\xi_p = P_{total}/V \tag{9}$$

**Table 4.** Comparison of the characteristics of the CADMP-FSPM machine and the DMP machine. THD, total harmonic distortion.

| Items | CADMP-FSPM | | DMP | |
|---|---|---|---|---|
| **Characteristics** | **Inner Machine** | **Outer Machine** | **Inner Machine** | **Outer Machine** |
| Magnitude of phase PM flux linkage (Wb) | 0.05 | 0.09 | 0.10 | 0.11 |
| THD of phase PM flux linkage (%) | 0.76 | 1.07 | 5.96 | 2.40 |
| Magnitude of phase EMF per turn (V) | 113.89 at 2400 r/min | 121.04 at 580 r/min | 135.80 at 2400 r/min | 137.83 at 2500 r/min |
| THD of phase EMF per turn (%) | 3.35 | 2.51 | 8.51 | 6.86 |
| Peak-to-peak cogging torque (Nm) | 2.76 | 15.8 | 18.75 | 17.71 |
| $T_{ave}$ (Nm) @ $J_{si}$ = 6.4 A/mm$^2$ $J_{so}$ = 5 A/mm$^2$ | 168.95 | 432.04 | 138.76 | 323.93; 398.44, (drive shaft) |
| Peak-to-peak electromagnetic torque $T_{ripple}$ (Nm) | 9.97 | 25.28 | 16.35 | 16.96 |
| $T_{ripple}$ (%) | 5.90 | 5.85 | 11.78 | 5.23 |
| $L_{aa}$ (mH) | 0.1818 | 0.5289 | 0.2393 | 0.3778 |
| $M_{ab}$ (mH) | 0.088 | 0.2471 | 0.0017 | 0.1189 |
| $M_{ac}$ (mH) | 0.088 | 0.2452 | 0.0016 | 0.1178 |
| Power (kW) | 42.20 | 26.23 | 34.67 | 48.45 |
| Total power (kw) | 68.43 | | 83.12 | |
| Power density (kw/m$^3$) | 5559.44 | | 6757.72 | |

### *4.5. Efficiency*

The efficiency analysis of the proposed CADMP-FSPM machine-based E-CVT system operated in different modes is a rather complicated problem. For the CADMP-FSPM machine, the inner FSPM machine operates as a generator most of the time; however, for the outer FSPM machine, it can operate as a generator or traction motor according to the situation. However, for the DMP machine, both the inner machine and the outer machine would operate as generators or traction motors simultaneously.

In addition, the outer rotor is shared by the inner and the outer machines, which means two machines are coupled with each other; thus, it is very difficult to investigate the efficiency of the DMP machine when both the inner and outer machines are operating. Hence, for comparing the efficiencies of the two machines, the efficiency maps of the outer and inner machines in different modes are investigated individually. It is worth noting that the inner FSPM machine of the CADMP-FSPM machine operates as a generator most of the time, and only in the engine cranking mode will the inner FSPM machine operate as a traction motor to start the ICE. Therefore, for the inner FSPM machine, only the efficiency under the generating mode is analyzed. The efficiency of the machine under generating and traction modes can be calculated respectively as follows [20]:

$$\eta_g = \frac{P_{out}}{P_{in}} = \frac{T_m\omega_m - p_{copper} - p_{core} - p_{PM} - p_{mec} - p_{stray}}{T_m\omega_m} \tag{10}$$

$$\eta_t = \frac{P_{out}}{P_{in}} = \frac{T_m\omega_m}{T_m\omega_m + p_{copper} + p_{core} + p_{PM} + p_{mec} + p_{stray}} \tag{11}$$

where $\eta_g$ and $\eta_t$ are the efficiency in generation and traction modes, respectively, $T_m$ and $\omega_m$ are the mechanical torque and mechanical rotation speed of the machine, respectively, and $p_{copper}$, $p_{core}$, $p_{PM}$, $p_{mec}$ and $p_{stray}$ are copper loss, core loss, PM eddy current loss, mechanical loss and stray loss, respectively.

The copper loss $p_{copper}$ can be expressed as:

$$p_{copper} = mI_p^2R_p \tag{12}$$

where $m$ is the phase number, $I_p$ is the root mean square (RMS) phase current and $R_p$ is the phase resistance of armature windings.

The core loss can be expressed as [21]:

$$p_{core} = k_e f^2 B_m^2 + k_h f B_m^2 \tag{13}$$

where $f$ is the frequency of sinusoidal alternating flux density, $B_m$ is the amplitude of flux density and $k_e$ and $k_h$ are eddy current and hysteresis loss coefficients, respectively.

The losses of the power electronic circuits are associated with the switching frequency of the power devices nonlinearly, which is relative to the turn-on losses and switching losses. Normally, the losses of the power electronics circuits can be measured by a power analyzer during experiments on a prototype machine according to the differences between input DC-side and out AC-side electric powers.

The PM eddy current loss $p_{PM}$ can be predicted by 2D FEA.

At the rated operation point, the distributed power loss of the proposed system by 2D FEA can be illustrated as Table 5, where copper loss, PM eddy loss and core loss are 40%, 23% and 37%, respectively.

**Table 5.** Percentage of the distributed power loss of the CADMP-FSPM machine.

| Item | PM Eddy Loss | Core Loss | Copper Loss |
|---|---|---|---|
| Percentage | 23% | 37% | 40% |

It is worth noting that the mechanical loss and stray loss cannot be predicted directly by FEA and are negligible compared to copper and core loess. However, the mechanical loss can be measured by open-circuit experiments at different speeds, and the stray loss is regularly 0.5% to 1% of the output power.

The efficiency maps in the traction and generating modes of the inner and outer machines of both CADMP-FSPM and DMP machines are shown in Figure 11a–g, In order to obtain accurate results, for the CADMP-FSPM or DMP machine, one of the inner or outer machines is at a standstill when the other machine is operating. It should be noted that for both inner machines, the operation speed is related to the ICE, which works at the optimal FCP, so both inner machines work only in the constant torque area. As can be seen, whether in traction or generating modes, the efficiency of both the inner and outer machines of the DMP machine is a little higher than that of the CADMP-FSPM machine, since the CADMP-FSPM machine has a higher frequency due to the larger pole pair number and larger slot areas.

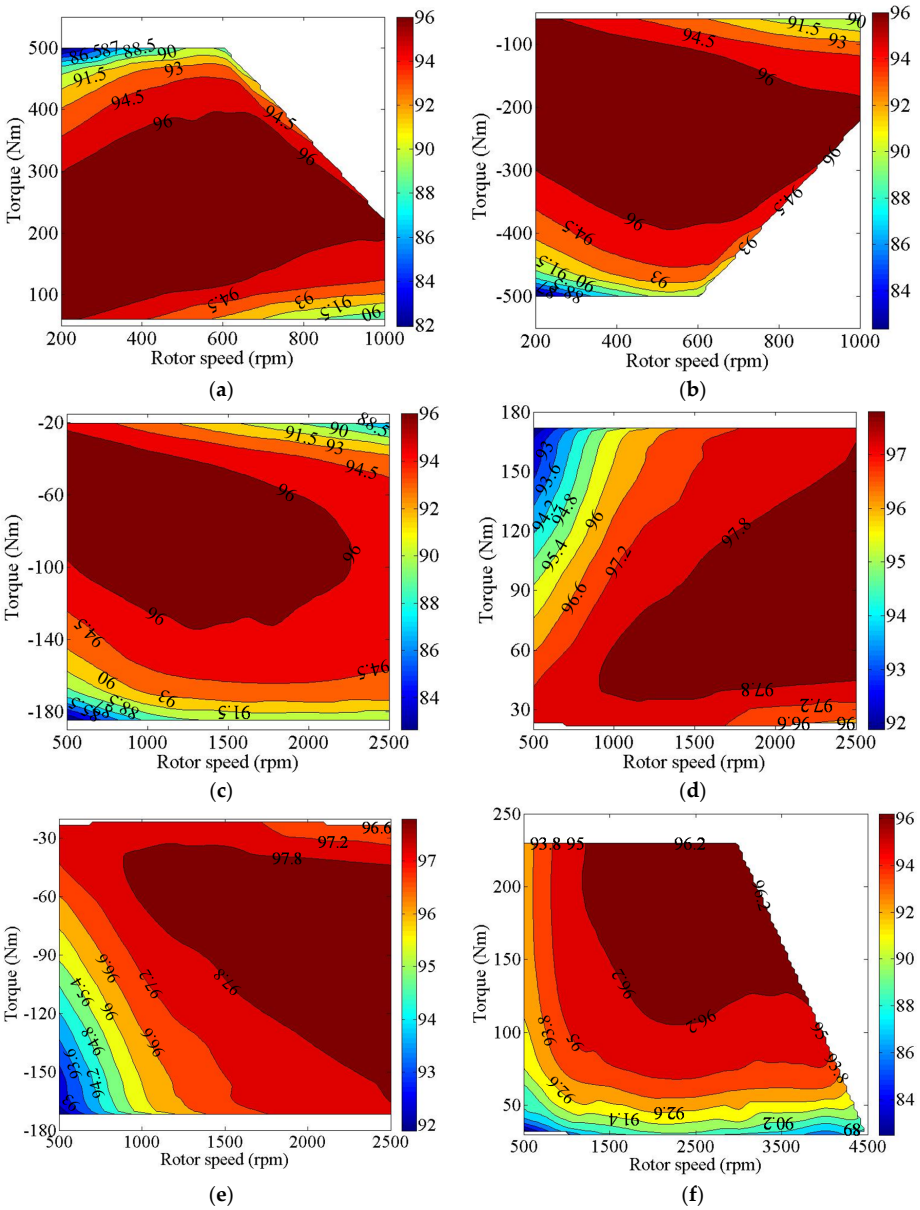


**Figure 11.** *Cont.*

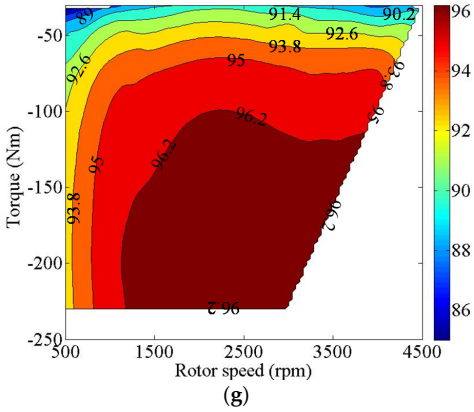


**Figure 11.** Efficiency maps of two machines. (**a**) Outer FSPM machine in traction mode; (**b**) Outer FSPM machine in generating mode; (**c**) Inner FSPM machine in generating mode; (**d**) Inner machine of the DMP machine in traction mode; (**e**) Inner machine of the DMP machine in generating mode; (**f**) Outer machine of the DMP machine in traction mode; (**g**) Outer machine of the DMP machine in generating mode.

## 5. Conclusions

In this paper, a novel co-axial dual mechanical ports flux switching permanent magnet machine is proposed and analyzed, where brushes, slip rings and reduction gears are removed. The topologies, operation modes, control system and electromagnetic performance of the CADMP-FSPM machines are introduced and analyzed. Then, a prototype with 12 inner stator slots/10 inner rotor poles and 12 outer stator slots/22 outer rotor poles is designed and optimized by 2D FEA. Finally, the performances of the CADMP-FSPM machine and a conventional DMP machine having the same volume designed for the practical application of the Toyota Prius are compared, and the results indicate that the CADMP-FSPM machine has advantages over the DMP machine, including elimination of brushes and slip rings, improved thermal dissipation conditions for the inner rotor, direct-driven operation, more flexible modes, lower cogging torque and torque ripple, lower THD values of the phase PM flux linkage and phase EMF and higher torque output capability, although the efficiency and the power density of the CADMP-FSPM machine are slightly lower than those of the DMP machine. Hence, the CADMP-FSPM machine can be a promising candidate and suitable for the E-CVT system in HEV applications. A further experimental validation is ongoing and will be reported soon.

**Acknowledgments:** This work was supported by the 973 Program of China (2013CB035603), the National Natural Science Foundation of China (51177013, 51322705), the Technology R&D Program of Jiangsu Province (BE2013880, BY2012195) and the "333 Talents Project" of Jiangsu Province.

**Author Contributions:** Wei Hua provided the idea of the CADMP-FSPM machine based E-CVT system, guidance and supervision; Ling Kang Zhou implemented the research, performed the optimization and finite-element analysis of the CADMP-FSPM machine and wrote the paper. All authors have contributed significantly to this work.

**Conflicts of Interest:** The authors declare no conflict of interest.

## References

1. Eriksson, S.; Sadarangani, C. A four-quadrant HEV drive system. In Proceedings of the 56th IEEE Vehicular Technology Conference, Vancouver, BC, Canada, 24–28 September 2002; Volume 3, pp. 1510–1514.
2. Hoeihmakers, M.J.; Ferreira, J.A. The electrical variable transmission. *IEEE Trans. Ind. Appl.* **2006**, *42*, 1092–1100. [CrossRef]

3. Cui, S.; Huang, W.; Cheng, Y.; Ning, K.; Chan, C.C. Design and experimental research on induction machine based electrical variable transmission. In Proceedings of the IEEE Vehicle Power and Propulsion Conference, Arlington, TX, USA, 9–12 September 2007; pp. 231–235.
4. Zheng, P.; Liu, R.; Qian, W.; Zhao, J. Magnetic coupling analysis of four-quadrant transducer used for hybrid electric vehicles. *IEEE Trans. Magn.* **2007**, *43*, 2597–2599. [CrossRef]
5. Xu, L. Dual-mechanical-port electric machines—A new concept in design and analysis of electric machines. In Proceedings of the IEEE Industry Industry Applications Conference, Annual Meeting, Hong Kong, China, 2–6 October 2005; Volume 4, pp. 2828–2834.
6. Niu, S.; Ho, S.L.; Fu, W.N. Design of a novel electrical continuously variable transmission system based on harmonic spectra analysis of magnetic field. *IEEE Trans. Magn.* **2013**, *49*, 2161–2164. [CrossRef]
7. Mo, L.H.; Quan, L.; Zhu, X.Y.; Chen, Y. Comparison and analysis of flux-switching permanent-magnet double-rotor machine with 4QT used for HEV. *IEEE Trans. Magn.* **2014**, *50*, 8205804. [CrossRef]
8. Cui, S.; Cheng, Y.; Chan, C.C. A basic study of electrical variable transmission and its application in hybrid electric vehicle. In Proceeding of the IEEE Vehicle Power and Propulsion Conference, Windsor, UK, 6–8 September 2006; pp. 1–4.
9. Hua, W.; Wu, Z.Z.; Ke, H.B.; Cheng, M. A Kind of Compromised Flux-Switching Permanent-Magnet Machine. China Patent 201210274466.1, 19 December 2012.
10. Xiang, Z.X.; Quan, L.; Zhu, X.Y.; Wang, L. A brushless double mechanical ports permanent magnet motor for plug-in HEVs. *IEEE Trans. Magn.* **2015**, *51*, 8111104. [CrossRef]
11. Fei, W.; Luk, P.C.K.; Shen, J.X.; Wang, Y.; Jin, M.; Jin, M. A novel permanent-magnet flux-switching machine with an outer-rotor configuration for in-wheel light traction applications. *IEEE Trans. Magn.* **2012**, *48*, 1496–1506. [CrossRef]
12. Wu, Z.Z.; Zhu, Z.Q. Analysis of air-gap field modulation and magnetic gearing effects in switched flux permanent magnet machines. *IEEE Trans. Magn.* **2015**, *51*, 8105012. [CrossRef]
13. Hua, W.; Cheng, M.; Zhu, Z.Q.; Howe, D. Analysis and optimization of back-EMF waveform of a flux-switching permanent magnet motor. *IEEE Trans. Energy Convers.* **2008**, *23*, 727–733. [CrossRef]
14. Fei, W.; Luk, P.C.K.; Shen, J.; Wang, Y. A novel outer-rotor permanent-magnet flux-switching machine for urban electric vehicle propulsion. In Proceeding of the IEEE International Conference on Power Electronics Systems and Applications, Hong Kong, China, 20–22 May 2009; Volume 3, pp. 1–6.
15. Chen, J.T.; Zhu, Z.Q.; Iwasaki, S.; Deodhar, R.P. Influence of slot opening on optimal stator and rotor pole combination and electromagnetic performance of switched-flux PM brushless AC machines. *IEEE Trans. Magn.* **2011**, *47*, 1681–1691. [CrossRef]
16. Hua, W.; Cheng, M.; Zhu, Z.Q. Design of flux-switching permanent magnet machine considering the limitation of inverter and flux-weakening capability. In Proceeding of the IEEE Industry Applications Society 41st Annual Meeting, Tampa, FL, USA, 8–12 October 2006; Volume 5, pp. 2403–2410.
17. Zhang, G.; Cheng, M.; Hua, W.; Dong, J. Analysis of the oversaturated effect in hybrid excited Flux-Switching machines. *IEEE Trans. Magn.* **2011**, *47*, 2827–2830. [CrossRef]
18. Wang, Y.; Jin, M.J.; Fei, W.Z.; Shen, J.X. Cogging torque reduction in permanent magnet flux-switching machines by rotor teeth axial pairing. *IET Electr. Power Appl.* **2010**, *4*, 500–506.
19. Bianchi, N.; Bolognani, S. Design techniques for reducing the cogging torque in surface-mounted PM motors. *IEEE Trans. Ind. Appl.* **2002**, *38*, 1259–1265. [CrossRef]
20. Hendershot, J.R., Jr.; Miller, T.J.E. *Design of Brushless Permanent-Magnet Machines*; Motor Design Books: Venice, FL, USA, 2010; ISBN: 978-0-9840687-0-8.
21. Zhu, S.; Cheng, M.; Dong, J.N.; Du, J. Core loss analysis and calculation of stator permanent-magnet machine considering DC-Biased magnetic induction. *IEEE Trans. Ind. Electron.* **2014**, *61*, 5203–5212. [CrossRef]